Effect of Continuous Stream and Agitator Type on CFSTR Mixing State

ARTICLE *in* INDUSTRIAL & ENGINEERING CHEMISTRY RESEARCH · JUNE 2006

Impact Factor: 2.59 · DOI: 10.1021/ie0600691

3 AUTHORS, INCLUDING:

Paul P Mavros
Aristotle University of Thessaloniki
47 PUBLICATIONS **708** CITATIONS

Effect of Continuous Feed Stream and Agitator Type on CFSTR Mixing State

Kostas Samaras, Paul Mavros,* and Dimitris Zamboulis

Department of Chemistry, Aristotle University, GR-54124 Thessaloniki, Greece

The hydrodynamics of a continuous-flow stirred tank reactor (CFSTR) have been studied through RTD measurements, visual tracing, and CFD simulations, for an axial-flow and two radial-flow impellers (Mixel TT and Rushton and NS turbines), to investigate how the combination of impeller choice and operating conditions (flow rates, agitator speed) affect the vessel hydrodynamics and flow nonideality. The portion of the total vessel volume being perfectly mixed decreases considerably as the vessel utilization is forced by decreasing the vessel retention time; at the same time the amount of feed bypassing/short-circuiting increases, too, especially in the case of axial-flow impellers. Qualitative and quantitative results are obtained, leading to conclusions about the suitability of particular impeller−vessel configuration combinations.

Introduction

A large corpus of chemical engineering research deals with various aspects of agitated vessel hydrodynamics, and several books have been published related to their use.[1−5] However, attention is usually devoted to the choice of the impeller, the required power, and various other technical details; little space has been devoted to the effects of the various design and process variables on the operation of continuous-flow stirred tank reactors (CFSTRs), especially vessel hydrodynamics and their nonideal flow characteristics, and the literature is scant.[6−10] Some indications were given by Gray[11] and by Berresford et al.,[12] but even more recent publications[13−15] give few or no details about their operation. In theory, CFSTRs are considered as perfectly mixed; it is however recognized[16] that, in reality, the retention time for some of the feed might be either shorter or longer than designed, because of bypassing and/or dead zones and that it may be possible to rectify this vessel pathology by an appropriate modification of "mixing intensity" and/or of the vessel configuration, in terms of inlet and outlet positions.

The purpose of the present work was to investigate experimentally how the vessel configuration, the choice of the impeller, and the operating conditions influence the stirred tank operation, and more precisely, what part of the total volume may be considered as well mixed, and what parts of the feed stream are thoroughly mixed or bypass the mixed volume, in relation to the above-mentioned variables. Residence time distribution measurements, direct visualizations using a suitable tracer, and numerical simulations using a commercial CFD code (CFX) yielded useful qualitative and quantitative information, which are used to suggest the mixing state and vessel bypass, for each tank−impeller configuration.

Mixing State and Flow Nonideality of CFSTRs

In a stirred tank, the rotation of the impeller induces a primary circulation (and possibly a secondary circulation, too). In the case of axial-flow impellers in both their up- or down-pumping, a single toroidal loop is thus formed around the impeller, and LDV measurements have indicated that the upper region of the vessel, away from the main circulation loop, is often poorly mixed.[17,18] In the case of radial-flow impellers, a double-toroidal flow pattern is established in the vessel. A novel radial-flow impeller ("NS" turbine) was found to induce a similar but inverse flow pattern, with liquid being sucked in from the side of the impeller and being pumped out from its bottom and top sides, with advantageous power and flow characteristics.[19]

Various studies have reported on the stirred tank hydrodynamics, in terms of flow patterns induced by the impellers, most of them referring to batch conditions (see, for example, the review of Nere et al.[20]), where the most important entity is the batch homogenization or mixing time (t_{mix}). Ruszkowski[21] published a simple correlation using results for a variety of agitators, relating t_{mix} to the vessel and impeller dimensions and the impeller power number. In its revised form,[22] it takes into account the time necessary for achieving 95% of the desired homogeneity:

$$Nt_{mix,95} = \alpha(Po)^{-1/3}\frac{T^{1.5}H^{0.5}}{D^2}, \quad \alpha = 5.20 + 0.52s, \quad s = 1, 2, 3 \quad (1)$$

where s depends on the confidence level required.

Introducing a continuous liquid stream in the stirred vessel affects its operation in various ways, which are also related to the internal vessel geometry and the choices of impeller and of the inlet and outlet positions. Previous studies identified the effects of the continuous through-flow by LDV measurements,[23−25] showing how the feed stream jet influenced the velocities in various regions in the vessel. The liquid stream is often fed at the top of the vessel, because of ease of operation; sometimes, the stream is introduced with a dip tube very close to the agitator so that the liquid may be introduced directly into the agitator suction stream. In chemical process vessels, liquid is often withdrawn from the bottom of the vessel, but sometimes from the top, by overflowing, too. Therefore, the choice of these locations may be crucial for the process.[26]

In CFSTRs, the principal hydrodynamic variable is the residence time distribution (RTD) of the liquid stream and its mean (τ). Levenspiel[27] discussed the various nonideal flow situations that may arise: on one hand, not all the volume of the stirred tank may be considered as well mixed, and on the other hand part of the feed stream might not be mixed with the mixed liquid in the vessel, bypassing or short-circuiting it and flowing directly into the tank outlet.

The operator of a CFSTR faces several questions: how should he choose the feed flow rate, the type of agitator to be used, and the inlet and outlet positions? How do these affect the

* To whom correspondence should be addressed. Fax +30-2310-997759. E-mail pmavros@chem.auth.gr.

10.1021/ie0600691 CCC: $33.50
Published on Web 05/19/2006

mixing state of the vessel contents and/or the extent of bypassing or short-circuiting? To the best of the authors' knowledge, very little information has been published in the open literature regarding what level of nonideal flow is acceptable or how this nonideality—dead regions, bypass, and/or short-circuiting—is taken into consideration. There seems that there is only an indication that the ratio of the mean residence time to the mixing time (τ/t_{mix}) should be about 10.[15,28] The present work attempts to obtain answers to some of these questions.

The simple exponential decay RTD (**E**) is too simple for analyzing nonideal flow situations. A wide variety of models have been proposed to deal with various hydrodynamic situations; among them, the one proposed by Cholette and Cloutier[29] remains, after so many years, as the simplest and still robust and useful one. In its most complete form, it accounts for regions with plug-flow characteristics (V_{plug}), dead volumes (V_{dead}), and bypassing or short-circuiting ($Q_{Lb} = Q_L - Q_{La}$), in addition to the perfectly mixed zone (V_{mix}). The exponential decay part of the curve is given by the following equation:

$$\mathbf{E}_{CC} = \begin{cases} 0 & 0 \le t < \dfrac{V_{plug}}{Q_L} \\ \left(\dfrac{Q_{Lb}}{Q_L}\right)\delta\left(t - \dfrac{V_{plug}}{Q_L}\right) + \left(\dfrac{Q_{La}}{Q_L}\right)\left(\dfrac{Q_{La}}{V_{mix}}\right) & \\ \quad \exp\left[-\left(\dfrac{Q_{La}}{V_{mix}}\right)\left(t - \dfrac{V_{plug}}{Q_L}\right)\right] & t \ge \dfrac{V_{plug}}{Q_L} \end{cases} \quad (2)$$

where Q_{La} is the part of the total feed flow rate (Q_L) being perfectly mixed. By fitting the model RTD ($\mathbf{E}_{CC}$) to experimental RTD data, it is possible to determine the values of the mixed volume and the bypass flow rate. Although eq 2 appears cumbersome, with four adjustable parameters, in practice it can be simplified, during numerical posttreatment of the RTD data: V_{plug} is calculated from the initial delay of the RTD, and the remaining unknowns are determined by taking into consideration only the exponential-like decay, which contains only two adjustable parameters, (Q_{La}/Q_L) and (Q_{La}/V_{mix}), from which Q_{La} and V_{mix} are easily found, and finally Q_{Lb} is also calculated.

The purpose of the present work is to determine how these results (V_{plug}, V_{dead}, Q_{Lb}, and V_{mix}) depend on various other process variables, to obtain valuable information about how mixing and vessel flow pathology depends on them.

Experimental Apparatus and Numerical Procedure

The Vessel. A cylindrical stirred vessel ($T = 190$ mm, $H_L = T$), with four baffles ($w_b = T/10$), made of Plexiglas and having a flat bottom, was used for all experimental measurements. An adjustable siphon system was used to maintain the liquid height in the stirred vessel constant throughout each experimental run. Tap water was used in all runs; its flow rate was measured and adjusted with a calibrated rotameter.

Three impellers (in all cases, $D = T/2$, $C = H/2$) were used (Figure 1): a radial-flow standard Rushton turbine ("RT"; $Po = 5.2$, $Fl = 0.75$), an axial-flow Mixel "TT" ($Po = 0.74$, $Fl = 0.67$),[18] and an inversed-radial-flow "NS" turbine ($Po = 1.0$, $Fl = 0.85$[30,31]).

A feed tube, with an i.d. of 10 mm, was used to feed the liquid stream into the CFSTR. In all cases, the feed stream was positioned so as to introduce the feed stream directly into the suction side of the impeller; thus, for the RT and the TT the tube was placed facing downward with its tip located 48 mm below the liquid surface (Figure 2a), corresponding to the

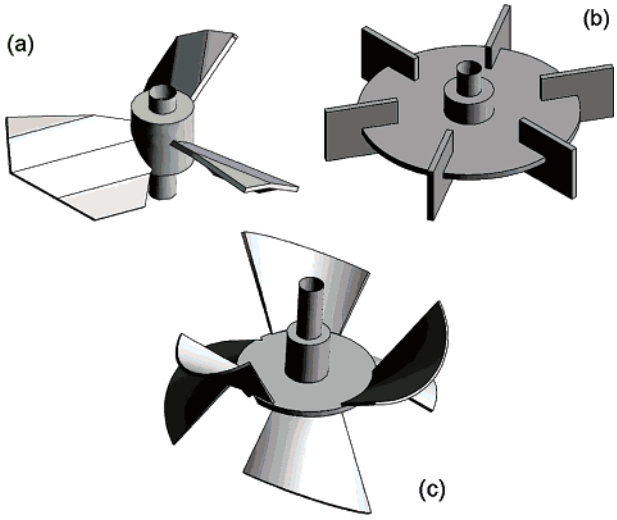

Figure 1. Impellers used in this work: (a) Mixel TT, (b) Rushton turbine, and (c) NS turbine.

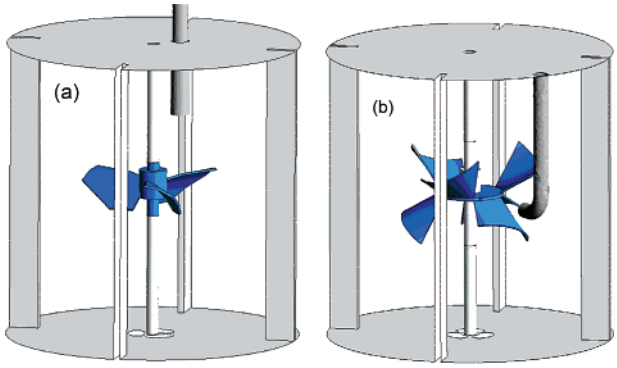

Figure 2. Experimental setup for (a) the axial-flow Mixel "TT" and the Rushton turbine and (b) the "NS" turbine.

configuration used previously for measuring the liquid velocities in the continuous-flow stirred vessel,[24,25] whereas for the NS, the tube was placed against the vessel wall, at the middle of the arc between two adjacent baffles, with its tip facing the disk of the impeller (Figure 2b) and its axis passing by the mid-disk plane. Both these regions have usually relatively low flow velocities; in the case of the "TT", the local velocity in the batch case was just 6.8% of V_{tip}, in the case of the Rushton turbine it was 14.2% of $V_{tip,}$ and for the NS turbine it was 4.7% of V_{tip}). The relation between the mean stream velocity at the tube tip and the impeller tip speed (u_L/V_{tip}) varies according to the rotation speed and the volumetric flow rate of the feed, from 0.23 in the case of a high rotation speed/low feed flow rate to 5.7 in the inverse case of low rotation speed/high feed flow rate.

In all cases, the vessel outlet was located at the center of the dished bottom; this is typical of a lot of industrial stirred vessels and chemical reactors, which are often equipped with a bottom drain valve.

Experimental Technique. A double-valve side tube was fitted to the feeding tube, as close to the vessel as possible. A small amount of tracer (an aqueous 3 M KCl solution) was poured in the side tube; with the simultaneous switch of the valves, the tracer was entrained by the feed stream and fed into the vessel, corresponding to an impulse input. The side tube with the double-valve setup means that the time necessary for the introduction of the tracer into the system flow was very short, being ≅0.15 s for the lowest feed flow rate, coming as close as practically possible to the ideal instantaneous impulse.

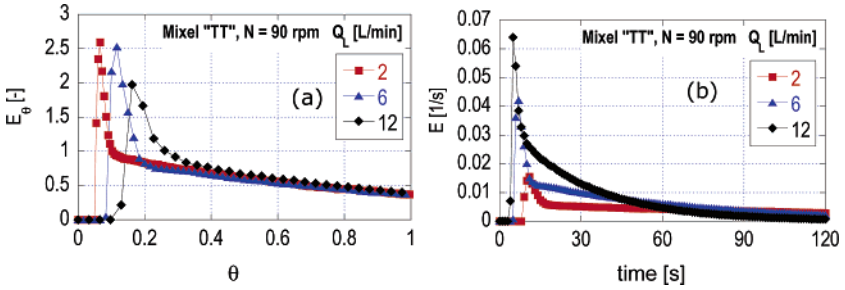

Figure 3. RTD curves for the axial-flow "TT" impeller ($\theta = t/\tau_{exp}$).

Other inputs could also be used, e.g., a step or a sinusoidal input; however, in our case, with the CSTR being fed directly from the mains tap, the impulse was judged to be more practical; the numerical posttreatment of the results, in the case of the impulse, is also more straightforward.

A through-flow conductivity cell was fitted to the exit tube, allowing for the continuous measurement of the exit stream conductivity; the conductivity meter (Crison GLP22) was connected to a PC, and the results—exit stream conductivity vs time—were logged with a frequency of 1 Hz. The total volume of the tube, from the switch to the feed tube tip, was approximately 56 cm^3, while the volume of the tube connecting the exit from the vessel to the conductivity cell was ~150 cm^3; the total tube volume corresponded to about 3.7% of the total liquid volume. At the lowest feed flow rate, i.e., the slowest tracer addition, the transit time of the tracer in the tubes was about 6 s.

Conductivity measurements were logged a period of time longer than 5 times the theoretical mean residence time, calculated each time from the liquid volume in the vessel and the feed flow rate.

Measurements of RTDs were performed for $N = 1.5$, 3, and 5 Hz (90, 180, and 300−240 rpm in the case of the Rushton turbine, because of surface aeration at higher rotation speeds) and for feed flow rates ranging from 3.33×10^{-5} to 2×10^{-4} $m^3\ s^{-1}$ (2−12 L min^{-1}). Three replications were measured for each experimental condition, and the RTDs showed excellent repeatability.

Numerical Postprocessing. The measurements were afterward numerically processed to obtain the RTD ($\mathbf{E}_{CC}$). The initial part of the RTD, with $\mathbf{E} = 0$, was used to determine the value of V_{plug}. Then, after a detailed inspection showed the extent of the bypass peak, the exponential decay part of the RTD and of eq 2 was used to determine (Q_{La}/Q_L) and (Q_{LA}/V_{mix}), and from these Q_{LA}, Q_{Lb}, V_{mix}, and V_{dead} were calculated. Brief initial tests for various values of (Q_{La}/Q_L) and (Q_{LA}/V_{mix}) showed that these two parameters affect the shape and position of the exponential decay curve in different ways; therefore, it was always possible to determine in a unique way the (Q_{La}/Q_L) and (Q_{LA}/V_{mix}) values for a particular experimental setup.

CFD Simulations. For the simulation of the flow in the continuous-flow stirred tank, the ANSYS-CFX (versions 5.7 and 5.7.1) commercial CFD code was used, while the geometries and meshes were designed with the ANSYS—Workbench and CFX—CAD2MESH tools. Because of the lack of symmetry, due to the inlet tube, the flow in the whole tank had to be simulated. The meshes comprised triangular 2D elements for the boundaries, prismatic elements in multiple layers for the y^+ regions and tetrahedral elements were used for the remaining volume.

The approach used to simulate the rotating impeller was the transient sliding mesh (SM) scheme. Two separate regions, the inner region of the rotating impeller and the outer region of the static reactor, were joined by an interface, taken 5 mm away from the impeller boundaries, in all three directions. For the calculations, a single PC unit was used (2.8GH, 1Gb RAM), and each run lasted between 18 and 30 clock hours.

Turbulence was modeled with the standard $k-\epsilon$ model; other models, like the $k-\omega$ or the shear stress transport (SST), were also tested but gave results similar to the $k-\epsilon$ model, especially in the critical near-wall flows, which were one of our major concerns, since the jet impinging on the impeller blades was the cornerstone of the simulations.

The total number of cells for the Mixel "TT" was ~700 000, corresponding to ~140 000 grid points, in ~145 000 grid points for the Rushton turbine and ~175 000 grid points for the NS impeller.

It should be noted that the simulation took care of all the actual geometric features, i.e., the impeller blades width was also modeled.

For the discretization of the flow equations, a first-order upwind scheme was applied. The walls were treated as no-slip wall boundaries, while the free liquid surface of the tank was modeled as a free-slip wall. The open surface at the tip of the inlet tube was an inlet with medium turbulence intensity (10%). The open surfaces at the bottom of the tank were assumed as openings with zero average static pressure.

Results and Discussion

1. RTD Results. RTD measurements were obtained with all three impellers for a wide range of feed flow rates so that the ratio of times τ/t_{mix} would extend from large ones to values less than 10, to determine how the vessel hydrodynamics are affected when the vessel usage is intensified, as seen by the increase in feed flow rate and the resulting decrease in τ.

Figure 3 presents typical RTD profiles for the axial-flow TT. The dimensionless plot (Figure 3a) is the usual way of presenting the results; in this case, however, this is misleading: as the liquid flow rate increases, the RTD shifts to the right, seeming to indicate less mixing and longer residence times, whereas we would expect that forcing more liquid through the vessel would result in shorter residence times and possibly more short-circuiting. The dimensional plot (Figure 3b) represents the results in a more acceptable—in this case—way: the short-circuiting peak appears earlier and becomes even sharper, as Q_L increases. Since conclusions drawn from dimensionless plots would thus be completely erroneous, the RTD profiles are deliberately presented in their dimensional form.

Figure 4 illustrates RTD profiles taken with all three impellers. The RTD for the axial-flow impeller ("TT") exhibits in most cases, especially at low agitation speeds and high Q_L values, a very distinct sharp initial peak, which is characteristic of part of the incoming liquid short-circuiting the vessel and flowing directly into the exit. As the liquid flow rate increases, the shape of the RTD changes; therefore, it is necessary to study

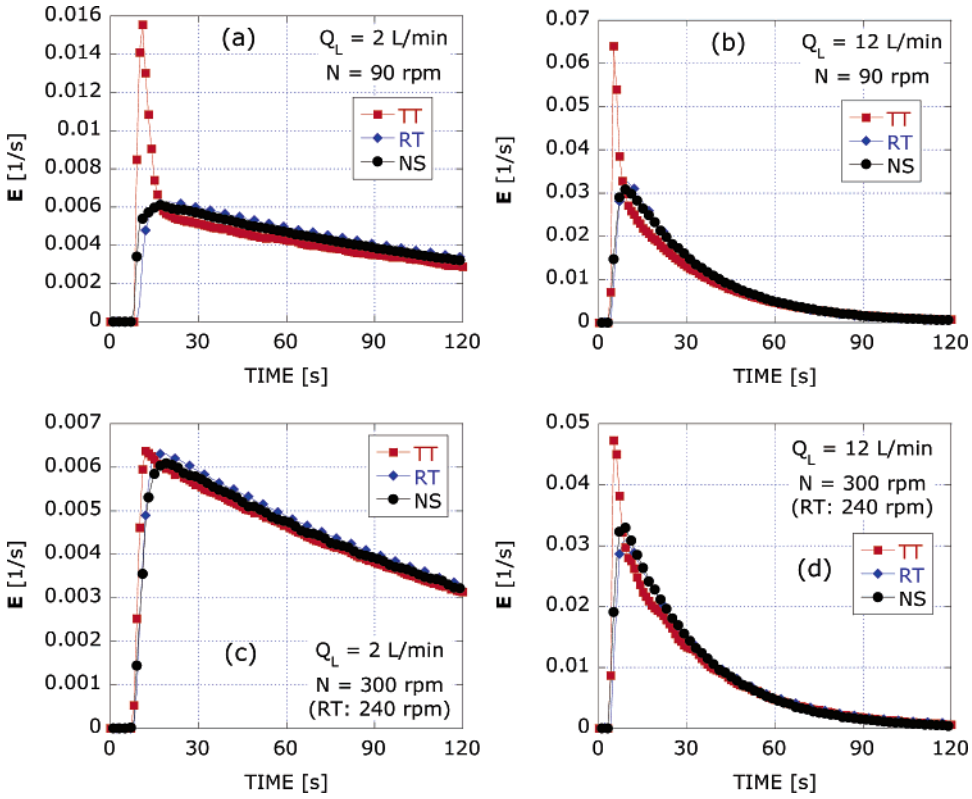

Figure 4. Comparison of RTDs for the three impellers tested for (a and c) $Q_L = 2$ L min^{-1} and (b and d) 12 L min^{-1} and for (a and b) $N = 1.5$ Hz (= 90 rpm) or (c and d) $N = 5$ Hz (= 300 rpm).

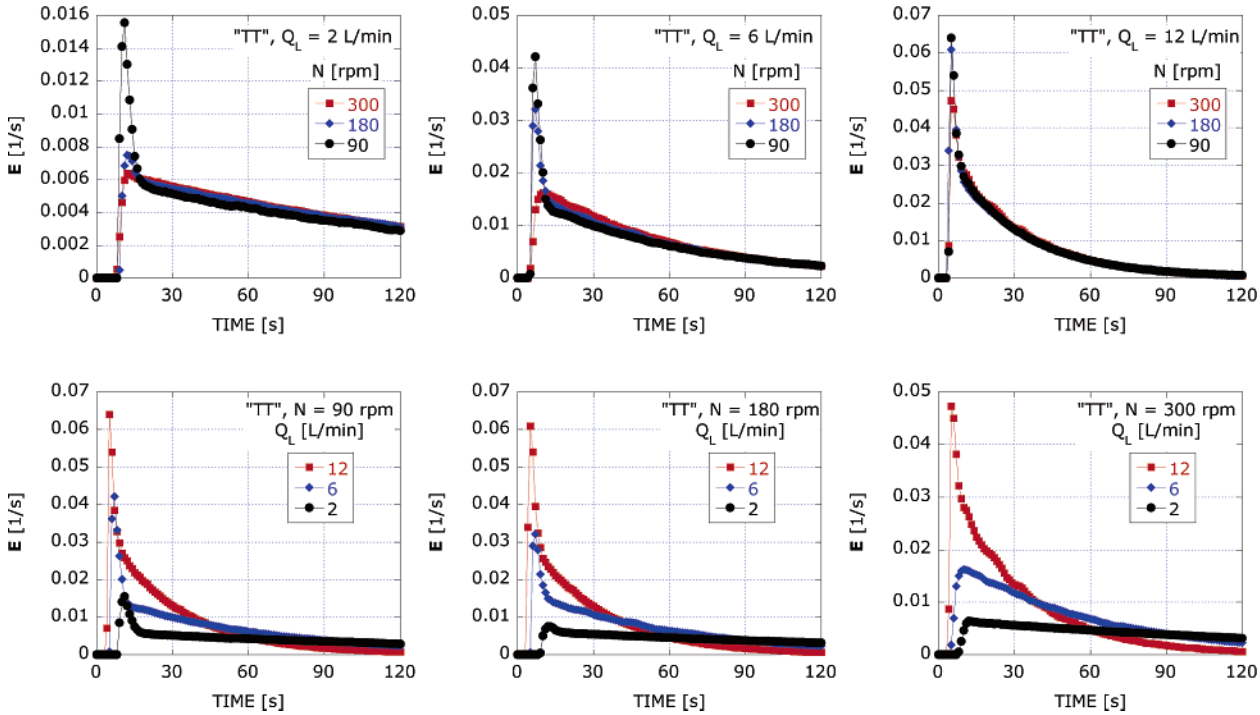

Figure 5. RTD curves for the axial-flow "TT" impeller.

in more detail the effects of the rotation speed and of the feed flow rate on the RTD. For a constant flow rate, as N increases, the short-circuiting peak diminishes but does not vanish (Figure 5); when Q_L is increased, the sharp peak eventually appears for all rotation speeds. The interaction of the feed stream and the impeller-pumped and circulating stream are more clearly visible, with the short-circuiting peak becoming gradually sharper, as Q_L increases, which means that more of the feed stream short-circuits the mixing vessel. Therefore, it appears that in the case of the axial-flow impeller, the engulfment of the incoming flow into the circulation inside the vessel depends both upon the feed flow rate and the rotation speed.

The RTD profile for the two radial-flow impellers, on visual inspection, were initially considered as being closer to the "perfectly mixed" condition, without any short-circuiting peak clearly visible. Plotting sample profiles from each experimental series in a dimensionless (θ, $\mathbf{E}_\theta$) plot, though, showed that even the radial RTDs departed from the perfectly mixed exponential

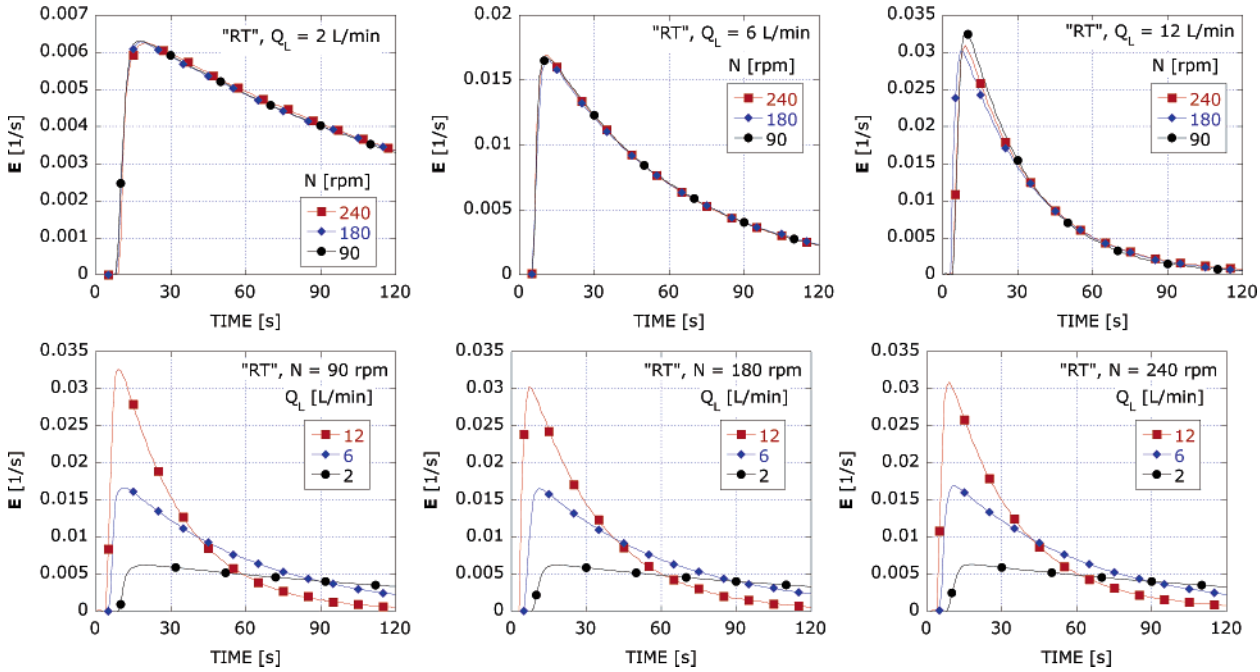

Figure 6. Comparison of RTD curves for the Rushton turbine.

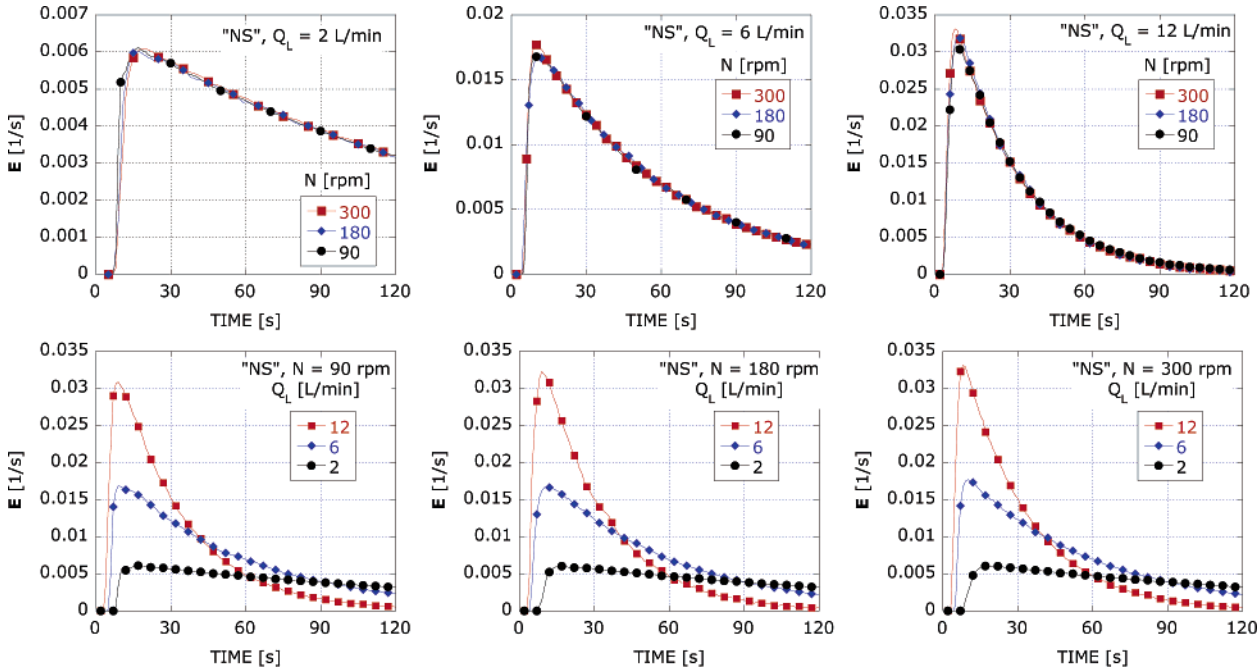

Figure 7. Comparison of RTD curves for the NS turbine.

decay. Their form did not vary much; typical RTD profiles are plotted and compared in Figures 6 and 7, in terms of increasing feed flow rate or agitator speed. Their analysis, though, showed that, even for the radial-flow impellers, it is necessary to take into account departures from the "perfectly mixed" ideal.

2. CFSTR Mixing State. Given the form of the RTDs, it was decided to analyze all the available results using the complete Cholette and Cloutier model (eq 2), since it is capable of giving estimates of all possible situations arising in a stirred vessel. The initial delay was used to estimate the percentage of the total volume (including the lead and exit tubes) exhibiting plug-flow-like (V_{plug}) flow features. The exponential part of all the RTD curves (all repetitions) was then examined, to determine whether the simple, completely mixed model could represent it accurately. With one exception, the simple exponential decay failed to represent correctly the form of the experimental profile, whereas eq 2 fitted it successfully—the presence of the (Q_{La}/Q_L) modifier making all the difference in the shape and position of the RTD curve. Thus, in all but one case, the RTD profiles yielded values for the bypassing flow rate, the dead volume region, and the remaining perfectly mixed region. The only exception was the case of the Rushton turbine at the lowest feed flow rate, where indeed no short-circuiting was observed, i.e., all the incoming feed was engulfed in its double-toroidal flow pattern.

Figure 8 present the results from fitting the Cholette and Cloutier model to the experimental RTDs. All plots indicate the mean value of the studied parameter with the corresponding minima and maxima, for the various experimental conditions tested. The results are plotted against the ratio of the two

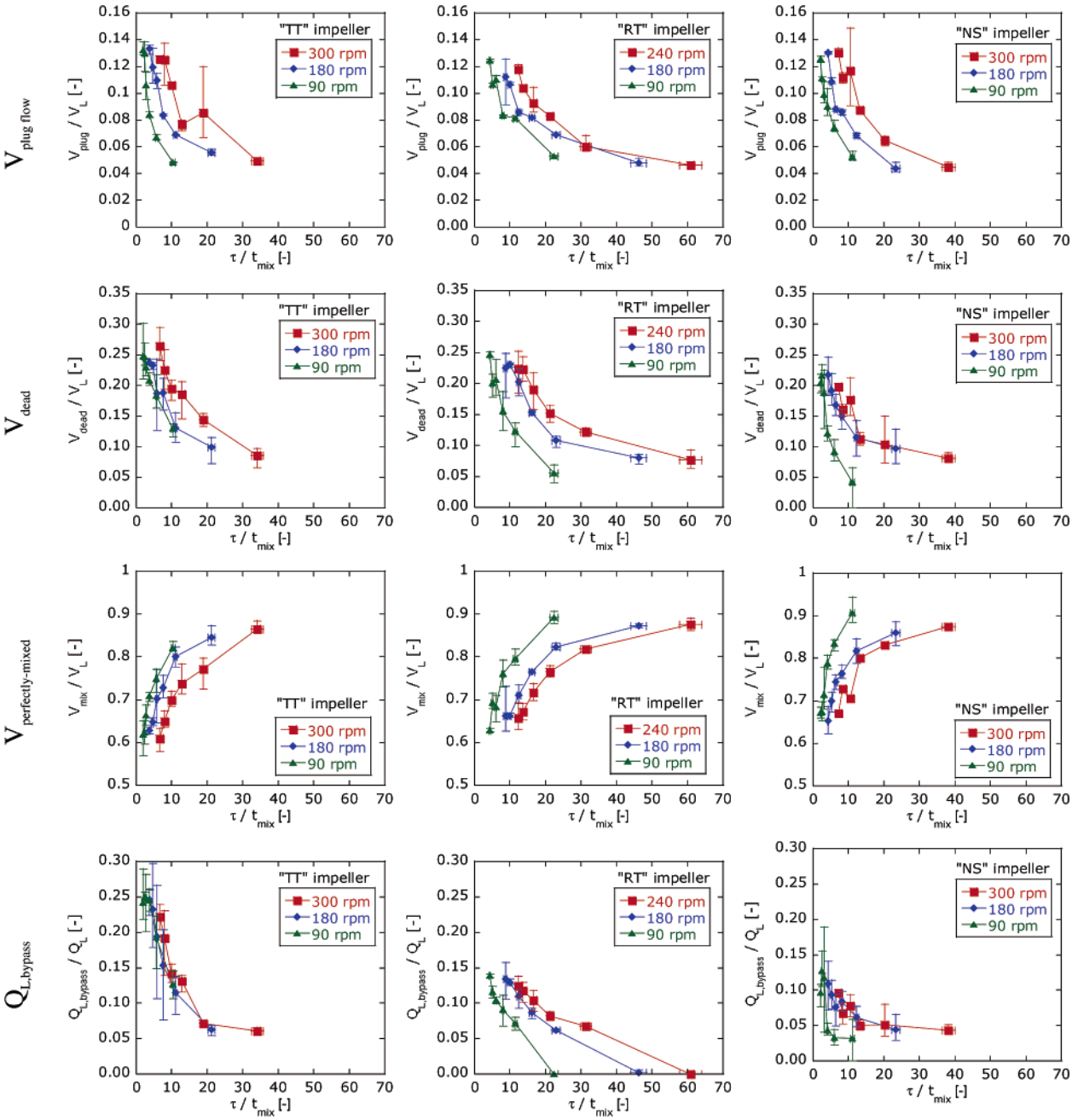

Figure 8. "Plug-flow" regions, "dead" volumes, perfectly mixed volumes, and bypassing/short-circuiting flow rates for the axial-flow Mixel "TT" and the radial-flow Rushton and "NS" turbines.

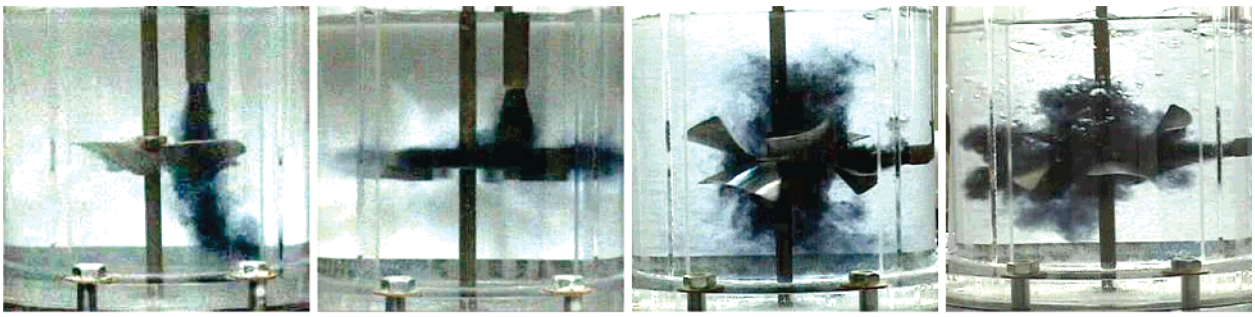

Figure 9. Visual tracing of flow patterns in continuous-flow stirred vessels: (a) TT, $N = 90$ rpm, $Q_L = 2$ L/min; (b) RT, $N = 90$ rpm, $Q_L = 2$ L/min; (c) NS, $N = 90$ rpm, $Q_L = 2$ L/min; (d) NS, $N = 90$ rpm, $Q_L = 12$ L/min.

characteristic times of the mixing process, i.e., the mean residence time and the mixing time, τ/t_{mix}; this ratio incorporates the effect of some of the major variables, i.e., the agitator type (through the impeller power number needed to calculate t_{mix}),

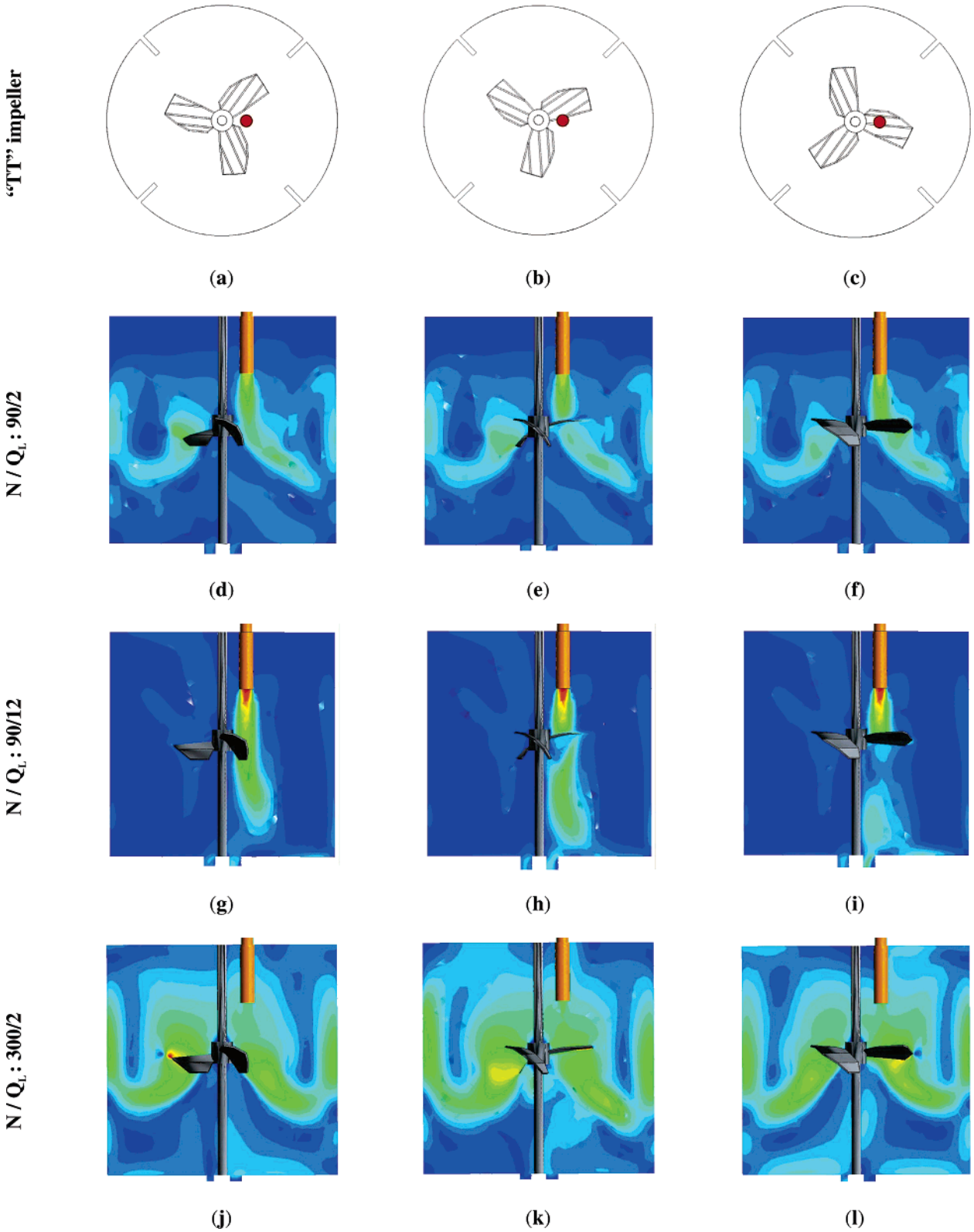

Figure 10. Calculated flow patterns in a CFSTR for an axial-flow "TT" impeller (flow rates [L/min] and rotation speeds [rpm] indicated on the side of the graphs; color scaling of velocities is not the same in all figures).

the rotation speed, and the feed flow rate. Since τ is related to Q_L and t_{mix} to Q_P, plotting the RTD results against the ratio τ/t_{mix} is equivalent to plotting them against the ratio of flow rates Q_P/Q_L. In that sense, these plots take into consideration the momentum of the two streams, too. It should be noted that the momentum of the feed stream could be altered also by choosing a different feed tube diameter; however, if a narrower tube was chosen, then the nonideality of the flow would be accentuated, whereas a larger tube with lower feed stream velocities would be rather impractical, especially if scaled up.

2.1. Plug-Flow Region. The percentage of the total vessel volume exhibiting a plug-flow behavior is similar in all cases; the slight differentiation in the curves is due only to the influence

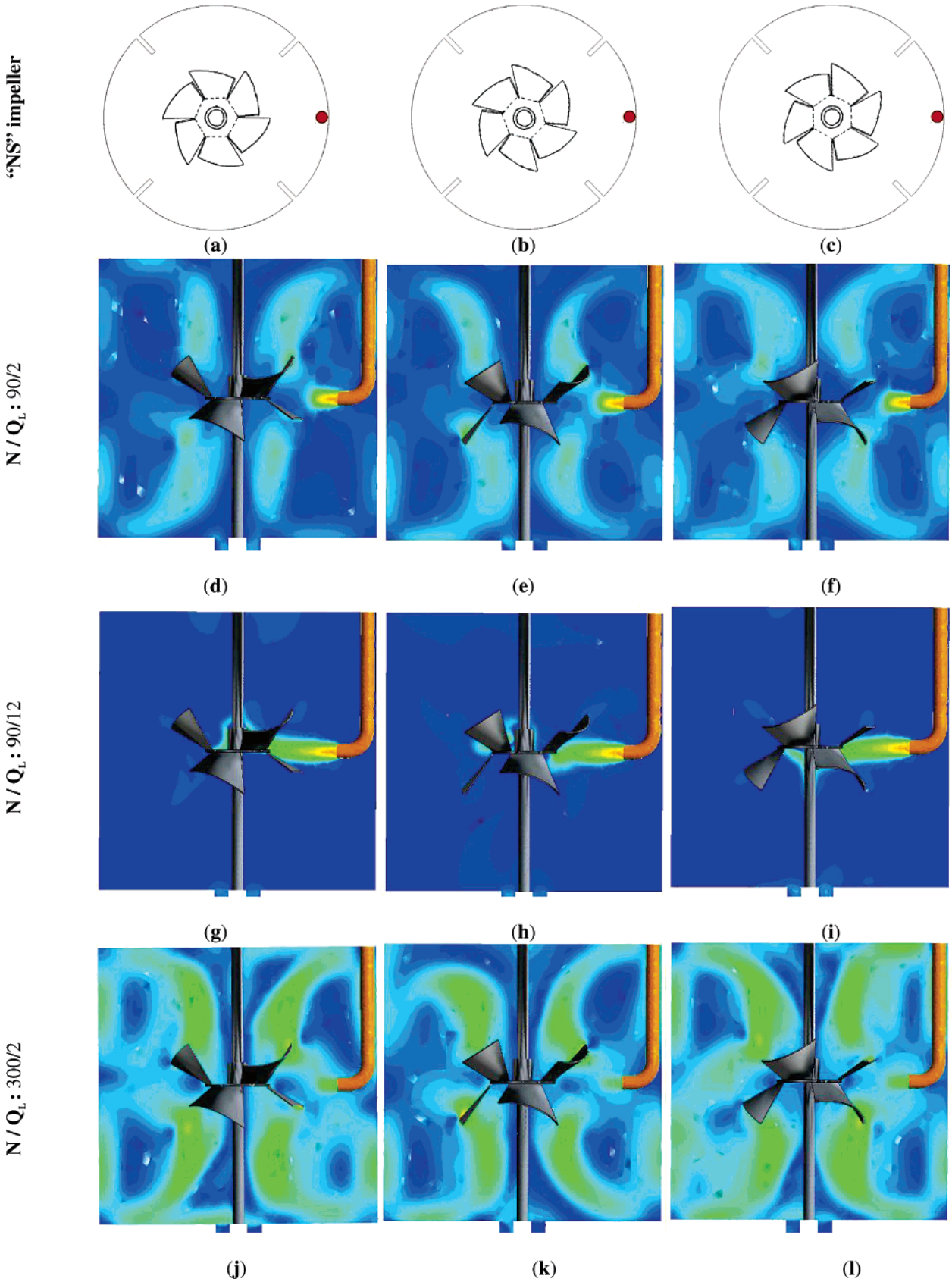

Figure 11. CFD simulations of CFSTR flow patterns for the "NS" turbine (flow rates [L/min] and rotation speeds [rpm] indicated on the side of the graphs; color scaling of velocities is not the same in all figures).

of the power number on the mixing time. From these results, one may conclude that a small part of the overall vessel volume—between 5% and 13%—should be considered as a plug-flow region for all modeling purposes, with the higher values corresponding to the vessel usage being intensified, i.e., with residence times becoming shorter.

2.2. Dead Volume. The analysis of the amount of dead volume for all three agitators yielded somewhat similar results.

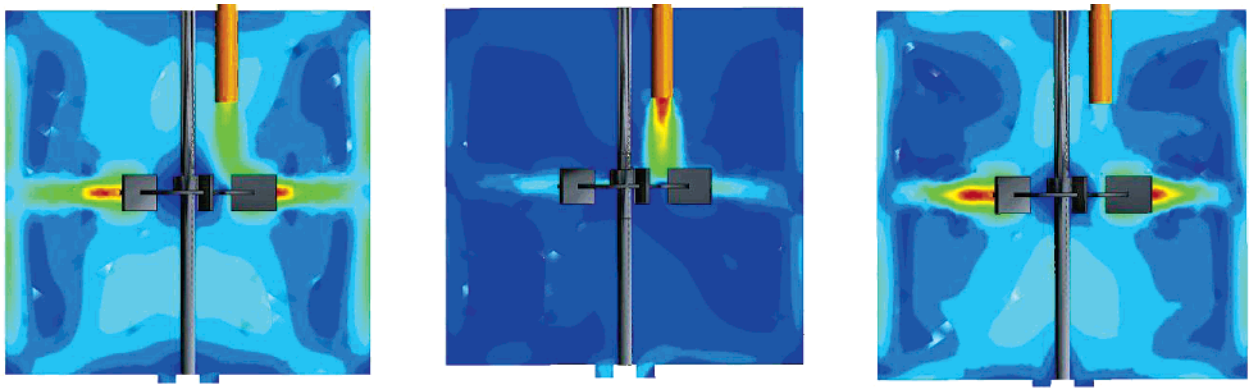

Figure 12. CFD simulations of CFSTR flow patterns for a Rushton turbine (flow rates [L/min] and rotation speeds [rpm] indicated beneath the graphs; color scaling of velocities is not the same in all figures).

As the ratio τ/t_{mix} decreases, especially below the literature-cited value of 10, the dead volume region increases to over 20% of the total vessel volume. Inversely, if one sets a particular value of V_{dead}/V_L as a maximum acceptable limit, this is reached faster as the agitator speed increases or as the power draw of the agitator increases, too. Therefore, the amount of dead volume depends again both on the type of agitator used as well as the operating conditions.

2.3. Perfectly Mixed Region. Once the plug-flow and the dead volume regions have been calculated, what is left of the total vessel volume corresponds to the perfectly mixed region of the stirred tank. Increasing the feed flow rate for a given agitator speed reduces the perfectly mixed zone in the stirred vessel, often considerably, well before the $\tau/t_{mix} = 10$ mark is crossed; the extent to which this reduction occurs depends also on the type of impeller and on its rotation speed, with faster rotation leading to a more reduced V_{mix}.

2.4. Bypass/Short-Circuiting. In terms of short-circuiting/bypassing, the type of impeller and flow pattern are decisive. At low feed flow rates, i.e., high τ values, the radial-flow RT and NS show very little short-circuiting/bypassing. In fact, for the RT, at the lowest feed flow rate, the best curve fitting was obtained for $Q_{La}/Q_L = 1$, which corresponds to zero Q_{Lb}, and only as Q_L increased, a small amount of bypassing/short-circuiting was observed. In the case of the axial-flow TT, on the other hand, short-circuiting was found to be considerable, especially for τ/t_{mix} decreasing below 10.

3. Visual Tracer Results. The RTD results were corroborated by visual observations with the use of an ink tracer (Figure 9). Focusing on the initial phase of the tracer entering the vessel, we may get an instantaneous glimpse of the flow pattern for the particular impeller. For the TT, both at low and high feed flow rates, the liquid jet passes through the impeller. The TT has a low solidity ratio ($\cong$0.39), and the jet intermittently crosses the impeller region or impinges on the blades and is diverted toward the empty space between two adjacent blades (Figure 9a). In the case of the RT, the jet is always obstructed by the presence of the turbine disk (Figure 9b), and the stream is therefore always diverted toward the sides of the impeller. In the case of the inverted-radial-flow NS, as long as the feed flow rate is low, the tracer is entrained by the main stream emerging from the upper and lower sides of the agitator (Figure 9c). When the feed is increased, eventually the stream passes through the impeller (Figure 9d), since its disk is not obstructing it, as in the case of the RT, and reaches the opposite vessel wall, from where it gradually spreads all over the vessel. Visual tracing, thus, confirmed that, in the case of the axial impeller and for this particular combination of feed and outlet points, some part of the feed stream—considerable in some cases—may short-circuit the main body of the mixed liquid in the vessel; on the other hand, the use of radial-flow agitators diminishes to some extent these cases of nonideal flow.

4. CFD Simulations. CFD calculations of the flow patterns for various feed flow rates also yielded results that illustrate the combined effect of the feed flow rate and of the agitator type and rotation speed on the flow inside the stirred vessel (Figures 10−12).

In the case of the axial-flow "TT" impeller, the instantaneous flow pattern results from the complex interaction between the position of the blades with respect to the feed tube and the volumetric flow rate of the feed stream. When the empty space between two adjacent blades is located beneath the tube (Figure 10a), the plunging jet may be seen reaching the impeller region, where it is deflected sideways into the stream pumped out by the impeller (Figure 10d). If the flow rate is increased (Figure 10g), the jet passes straight through the impeller region, reaching the bottom of the vessel, and a stream may be seen flowing directly into the vessel outlet, effectively short-circuiting the whole vessel. On the other hand, a low flow rate with a high rotation speed results in an apparently complete engulfment of the incoming stream into the liquid ejected by the rotating impeller (Figure 10j). When the impeller rotates so that the blade starts appearing beneath the feed tube (Figure 10b), the complex interaction between the incoming stream and the impeller region becomes more apparent: at low flow rates and low rotation speeds, the incoming jet is partially blocked by the blade and is diverted into the pumped out stream. The total blockage of the feed stream may be seen when the blade is positioned beneath the feed tube (Figure 10c), especially for the high flow rate (Figure 10h). At the highest rotation speed of 5 Hz (300 rpm), the circulation around the "TT" impeller appears very intense, and the passage of the blades beneath the feed tube only partially affects the flow pattern in the stirred vessel (Figure 10j−l).

A somewhat similar effect might have been expected in the case of the inverted-radial-flow "NS" turbine (Figure 11), because of the intermittent alternate blocking of the feed stream by the upper or lower blade, which results in the feed stream being directed regularly toward the upper or the lower part of the turbine (see Figure 1c and Figure 11a−c for the position of the feeding tube tip relative to the impeller, with the vertical tube positioned flush to the wall). However, the strong outgoing

stream from the upper and lower sides of the turbine seems to entrain most of the feed stream, even for the highest tested flow rate, and only at the highest flow rate the incoming jet may be seen reaching and then crossing the turbine (Figure 11g−i), for all three blade positions.

In the case of the Rushton turbine (Figure 12), the incoming stream is permanently blocked by the turbine disk; therefore, it has to be deflected sideways and is incorporated in the stream pumped out sideways by the turbine. The interaction between the feed flow rate and the impeller rotation results only in a change of velocity magnitudes, as seen by the differing coloring of Figure 12a−c, but otherwise no major change in the overall flow pattern is noticeable.

Discussion and Conclusions

Experimental RTD work, visual tracing, and CFD simulations have been used to study the complex interaction of the choice of agitator, vessel configuration, and operational variables and their influence on the hydrodynamics of a continuous-flow stirred tank and more specifically the nonideality of the flow in it. The results, for the tested configuration involving top-fed vessels with the liquid outlet located at the bottom of the vessel, indicate the following:

(i) A small portion of the overall liquid volume will correspond to plug flow ($4\% < V_{plug}/V_{total} < 14\%$); this increases with an increase in feed flow rate (corresponding to a reduction in the ratio of characteristic times τ/t_{mix}).

(ii) Another, more important portion of the total volume ($5\% < V_{dead}/V_{total} < 25\%$) will behave as dead volume; as the ratio τ/t_{mix} decreases, corresponding to more liquid being fed to the CFSTR and an intensification of the vessel usage, the dead volume percentage also increases to a considerable portion of the vessel volume.

(iii) Thus, the amount of liquid in the vessel volume considered as perfectly mixed drops substantially, to values below 80%, even reaching just 60% when the feed flow rate is increased.

(iv) Part of the feed flow rate short-circuits the vessel and flows directly into the outlet, without being mixed with the vessel contents. This short-circuiting flow is particularly important in the case of the axial-flow impeller, with $Q_{L,bypass}/Q_L > 10\%$ possibly due to its low solidity ratio, which allows the feed jet to flow intermittently through the impeller and reach directly the vessel outlet; in the case of radial-flow impellers, it is still present but to a smaller extent ($Q_{L,bypass}/Q_L < 10\%$), possibly because of the presence of disk obstructing the feed stream and directing it into the circulation loops.

Thus, it is evident that the nonideality of the flow in the CFSTR depends on the following:

(v) the type of agitator, with axial-flow agitators being responsible for an increase in nonideality;

(vi) the vessel configuration, especially the inter-related location of the feed and the outlet;

(vii) the feed flow rate, with an increase in flow rate—corresponding to a vessel usage intensification and a decrease in retention time—resulting in an increase in flow nonideality.

At this stage, it is neither possible to determine design limits nor to provide definitive recommendations. It appears only possible to increase the awareness of the operator/designer of CFSTRs that the design of a mixing system for a specific process requirement will follow a trial-and-error procedure:

(viii) First, a choice about the type of impeller to be used should be made, as well as its rotation speed.

(ix) Then, the feed flow rate should be selected, depending on overall process requirements.

The data of Figure 8 will then indicate the extent of flow nonideality that may be expected for such a system; it is then up to the operator/designer to decide whether this is acceptable or whether he/she should start again, possibly choosing other operating conditions or even a different agitator.

More work is necessary, and is currently being carried out, regarding alternative vessel feed and outlet combinations, as well as other impeller types.

Nomenclature

C = impeller clearance from the bottom of the tank (m)
D = impeller diameter (m)
$\mathbf{E}$ = residence time distribution (RTD) (s^{-1})
$\mathbf{E}_{CC}$ = Cholette and Cloutier model RTD (s^{-1})
$\mathbf{E}_\theta$ = dimensionless RTD
Fl = impeller flow number
H_L = liquid height in tank (m)
k = turbulent kinetic energy ($m^2\ s^{-2}$)
N = agitator rotation speed (Hz)
Po = impeller power number
Q_L = liquid feed volumetric flow rate ($m^3\ s^{-1}$)
Q_{La} = flow rate of stream entering mixed volume ($m^3\ s^{-1}$)
Q_{Lb} = flow rate of stream bypassing mixed volume ($m^3\ s^{-1}$)
Q_P = impeller-pumped volumetric flow rate ($m^3\ s^{-1}$)
s = variable (eq 1)
t = time (s)
t_{mix} = mixing time (s)
T = tank diameter (m)
u_L = feed flow velocity at the exit of the feeding tube ($m\ s^{-1}$)
u_z = axial liquid velocity in the tank ($m\ s^{-1}$)
V_L = total liquid volume in tank (m^3)
V_{dead} = dead volume (m^3)
V_{mix} = perfectly mixed liquid volume (m^3)
V_{plug} = plug-flow volume (m^3)
V_{tip} = impeller tip speed ($m\ s^{-1}$)
w_b = baffle width (m)

Greek letters

α = coefficient (eq 1)
θ = dimensionless time
τ = mean residence time (s)

Literature Cited

(1) Paul, E. L., Atiemo-Obeng, V. A., Kresta, S. M., Eds. *Handbook of Industrial Mixing—Science and Practice*; Wiley-Interscience: Hoboken, NJ, 2004.

(2) Nauman, B. *Handbook of Chemical Reactor Design, Optimization, and Scale-up*; McGraw-Hill: New York, 2002.

(3) Chhabra, R.; Richardson, J. F. *Non-Newtonian Flow in the Process Industries: Fundamentals and Engineering Applications*; Butterworth-Heinemann: Oxford, 1999.

(4) Harnby, N., Edwards, M. F., Nienow, A. W., Eds. *Mixing in the Process Industries*, 2nd ed.; Butterworth-Heinemann: Oxford, 1992.

(5) Rauwendaal, C., Ed. *Mixing in Polymer Processing*; Marcel Dekker: New York, 1991.

(6) Hubbard, D. W.; Patel, H. Hydrodynamic measurements for imperfect mixing processes: Newtonian fluids. *AIChE J.* **1971**, *17*, 1387−1393.

(7) Leitman, R. H.; Ziegler, E. N. Stirred tank reactor studies: Part 1: Mixing parameters. *Chem. Eng. J.* **1971**, *2*, 252−260.

(8) Burghardt, A.; Lipowska, L. Mixing phenomena in a continuous flow stirred tank reactor. *Chem. Eng. Sci.* **1972**, *27*, 1783−1795.

(9) Lipowska, L. The influence of geometric parameters on the ideal mixing range of liquid in a continuous flow stirred tank reactor. *Chem. Eng. Sci.* **1974**, *29*, 1901−1908.

(10) Magelli, F.; Pasquali, G.; Foraboschi, F. P.; Lelli, U. A note on the validity of perfect mixing as a model for continuous stirred tanks.

Proceedings of an International Symposium on Mixing, Mons, Belgium, Feb 21−24, 1978; Bruxelmane, M., Ed.; Faculté Polytechnique de Mons: Mons, Belgium, pp A2.1−11.

(11) Gray, J. B. Flow patterns, fluid velocities, and mixing in agitated vessels. In *Mixing. Theory and Practice*; Uhl, V. W., Gray, J. B., Eds.; Academic Press: New York, 1966; Vol. I, Chapter 4.

(12) Berresford, H. I.; Gibilaro, L. G.; Spikins, D. J.; Kropholler, H. W. Continuous blending of low viscosity fluids: an assessment of scale-up criteria. *Trans. Inst. Chem. Eng.* **1970**, *48*, T21−T27.

(13) Roustan, M.; Pharamond, J.-C.; Liné, A. Agitation. Mélange. Concepts théoriques de base. In *Génie des Procédés*; Techniques de l'Ingénieur: Paris, 1999; J3800, pp 1−22.

(14) Zlokarnik, M. *Stirring. Theory and Practice*; Wiley-VCH: Weinheim, Germany, 2001.

(15) Patterson, G. K.; Paul, E. L.; Kresta, S. M.; Etchells, A. W., III. Mixing and chemical reactions. In *Handbook of Industrial Mixing—Science and Practice*; Paul, E. L., Atiemo-Obeng, V. A., Kresta, S. M., Eds.; Wiley-Interscience: Hoboken, NJ, 2004; pp 782−867.

(16) Speight, J. G.; Özüm, B. *Petroleum Refining Processes*; Marcel Dekker: New York, 2001.

(17) Mavros, P.; Xuereb, C.; Bertrand, J. Determination of 3-D flow fields in agitated vessels by laser-Doppler velocimetry. Effect of impeller type and liquid viscosity on liquid flow patterns. *Chem. Eng. Res. Des.* **1996**, *74* (A6), 658−668.

(18) Aubin, J.; Mavros, P.; Fletcher, D. F.; Bertrand, J.; Xuereb, C. Effect of axial agitator configuration (up-pumping, down-pumping, reverse rotation) on flow patterns generated in stirred vessels. *Chem. Eng. Res. Des.* **2001**, *79* (A8), 845−856.

(19) Mavros, P.; Mann, R.; Vlaev, S. D.; Bertrand, J. Experimental visualization and CFD simulation of flow patterns induced by a novel energy-saving dual-configuration impeller in stirred vessels. *Chem. Eng. Res. Des.* **2001**, *79* (A8), 857−866.

(20) Nere, N. K.; Patwardhan, A. W.; Joshi, J. B. Liquid-phase mixing in stirred vessels: turbulent flow regime. *Ind. Eng. Chem. Res.* **2003**, *42*, 2661−2698.

(21) Ruszkowski, S. S. A rational method for measuring blending performance and comparison of different impeller types. In *Proceedings of the 8th European Mixing Conference*, Cambridge, U.K., Sept 21−23, 1994; I.Chem.E.: Rugby, UK, pp 283−291.

(22) Grenville, R. K.; Nienow, A. W. Blending of miscible liquids. In *Handbook of Industrial Mixing—Science and Practice*; Paul, E. L., Atiemo-Obeng, V. A., Kresta, S. M., Eds.; Wiley-Interscience: Hoboken, NJ, 2004; pp 507−542.

(23) Mavros, P.; Naude, I.; Xuereb, C.; Bertrand, J. Laser Doppler velocimetry in agitated vessels. Effect of continuous liquid stream on flow patterns. *Chem. Eng. Res. Des.* **1997**, *75A*, 763−776.

(24) Mavros, P.; Xuereb, C.; Foøt, I.; Bertrand, J. Investigation of flow patterns in continuous-flow stirred vessels by laser Doppler velocimetry. *Can. J. Chem. Eng.* **2002**, *80* (4), 591−600.

(25) Mavros, P.; Xuereb, C.; Foøt, I.; Bertrand, J. Investigation by laser Doppler velocimetry of the effects of liquid flow rates and feed positions on the flow patterns induced in a stirred tank by an axial-flow impeller. *Chem. Eng. Sci.* **2002**, *57*, 3939−3952.

(26) Hemrajani, R. R.; Tatterson, G. B. Mechanically stirred vessels. In *Handbook of Industrial Mixing—Science and Practice*; Paul, E. L., Atiemo-Obeng, V. A., Kresta, S. M., Eds.; Wiley-Interscience: Hoboken, NJ, 2004; p 352.

(27) Levenspiel, O. *Chemical Reaction Engineering*, 3rd ed.; John Wiley & Sons: New York, 1999.

(28) Trambouze, P. Réacteurs chimiques. Technologie. In *Génie des Procédés*; Techniques de l'Ingénieur: Paris, 1993; J4020, p 10.

(29) Cholette, A.; Cloutier, L. Mixing efficiency determinations for continuous flow systems. *Can. J. Chem. Eng.* **1959**, *37*, 105−115.

(30) Mavros, P.; Mann, R.; Vlaev, S. D.; Bertrand, J. Experimental visualization and CFD simulation of flow patterns induced by a novel energy-saving dual-configuration impeller in stirred vessels. *Chem. Eng. Res. Des.* **2001**, *79* (A8), 857−866.

(31) Vlaev, S. D.; Mavros, P.; Seichter, P.; Mann, R. Operational characteristics of a new energy-saving impeller for gas−liquid mixing. *Can. J. Chem. Eng*. **2002**, *80*, 653−659.

Received for review January 16, 2006
Revised manuscript received March 27, 2006
Accepted April 19, 2006

IE0600691